CJC Chinese Journal of Chemistry 中国化学 - An International Journal

For submission: https://mc.manuscriptcentral.com/cjoc
For published articles: https://onlinelibrary.wiley.com/journal/16147065

Concise Report

Cite this paper: *Chin. J. Chem.* **2021**, *39*, 1898—1904. **DOI: 10.1002/cjoc.202000675**

Bioinspired Activation of N_2 on Asymmetrical Coordinated Fe Grafted 1T MoS_2 at Room Temperature†

Jiaojiao Guo,[‡,a] Maoyu Wang,[‡,b] Liang Xu,[‡,c] Xiaomin Li,[‡,a,e] Asma Iqbal,[a] George E. Sterbinsky,[d] Hao Yang,[c] Miao Xie,[c] Jiantao Zai,*[,a] Zhenxing Feng,*[,b] Tao Cheng,*[,c] and Xuefeng Qian[a]

[a] *School of Chemistry and Chemical Engineering and State Key Laboratory of Metal Matrix Composites, Shanghai Jiao Tong University, Shanghai 200240, China*
[b] *School of Chemical, Biological, and Environmental Engineering, Oregon State University, Corvallis, OR 97331, USA*
[c] *Institute of Functional Nano and Soft Materials (FUNSOM), Jiangsu Key Laboratory for Carbon-Based Functional Materials and Devices, Soochow University, Suzhou, Jiangsu 215123, China*
[d] *Advanced Photon Source, Argonne National Laboratory, Argonne, IL 60431, USA*
[e] *Instrumental Analysis Center, Shanghai Jiao Tong University, Shanghai 200240, China*

Keywords

Monolayers | Redox chemistry | Electron transfer | Nitrogen fixation | 1T MoS_2

Main observation and conclusion

Inspired by the nitrogen fixation process on MoFe nitrogenase, asymmetrical coordinated Fe grafted onto 1T MoS_2 were successfully synthesized. The unique electron-rich structure with asymmetrical coordination made the 1T $Fe_{0.1}Mo_{0.9}S_2$ layered material actively react with water and dinitrogen at room temperature and atmosphere pressure. Subsequently, ammonia can be produced with a yield of ~800 μmol (NH_4^+) g^{-1} (12.5% yield in mole). The activation, fixation and reduction of dinitrogen were confirmed by isotopically labeled experiments. The location and the specific coordination environment of grafted Fe in Fe-Mo-S were further determined by X-ray absorption spectroscopy analysis. Our work demonstrates that the nitrogen fixation and reduction for ammonia at room temperature without any chemical and electrochemical assistance is distinctly different from traditional bionic-inspired nitrogen fixation process. The mechanism of the activation and reduction of N_2 was further investigated by density functional theory calculation and Raman spectra. Compared with 1T MoS_2, the enriched electron nature and asymmetrical coordination of Fe in Fe-Mo-S materials play a critical role in the bioinspired activation of N_2 at ambient condition.

Comprehensive Graphic Content

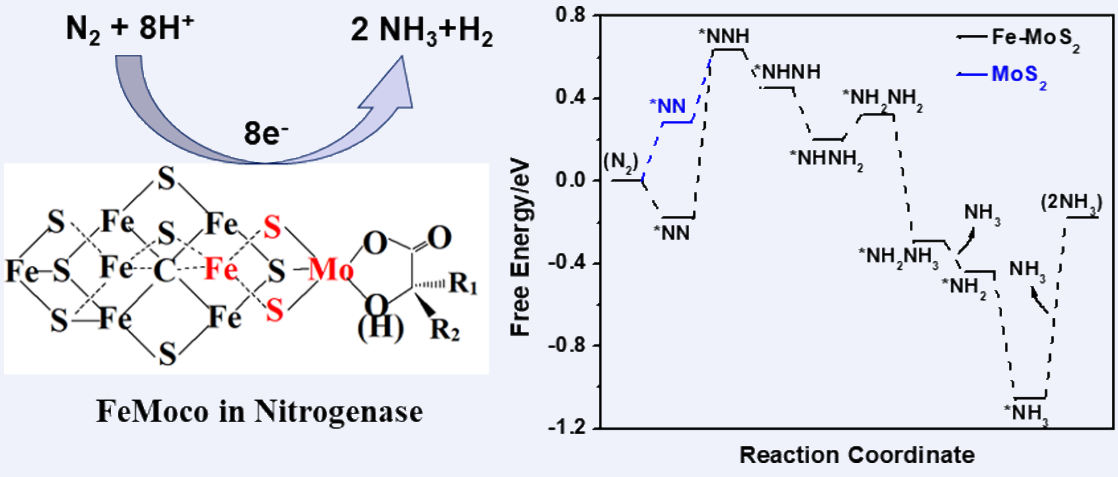

*E-mail: zaijiantao@sjtu.edu.cn; zhenxing.feng@oregonstate.edu; tcheng@suda.edu.cn
‡These authors contribute equally to this work.
† Dedicated to Professor Yitai Qian on the Occasion of His 80th Birthday.

View HTML Article | Supporting Information

Background and Originality Content

Nitrogen fixation is an extremely vital process that nourishes the life on earth.[1-2] Since the development of Haber-Bosch process (HBP) in 1900s, synthesis of ammonia at industrial scale has utilized the dinitrogen (N_2) that is rich in atmosphere (78% of the air). It significantly met the demand to produce chemical fertilizers, in turn supporting the population growth from 1.8 billion to 6.5 billion during the last hundred years.[3] However, the conversion of N_2 to ammonia requires harsh conditions like high pressure and temperature (~300 atm and 400—600 °C),[4] as the bond disassociation energy for N≡N is 945 kJ/mol.[5] In addition, the purification of nitrogen and hydrogen also consumes lots of energy, which, consequently raises 2% of global energy consumption and 2%—3% of global CO_2 emission.[1-2,6] Therefore, exploring N_2 activation and reduction strategies at ambient conditions (*i.e.*, room temperature and atmospheric pressure) is crucial to reduce the energy consumption and improve the efficiency of ammonia production.

In nature, enzymes accomplished more than 50% of dinitrogen fixation and conversion at room temperature and atmospheric pressure.[7] In the biological processes (Scheme A1), electron transfer is associated when N_2 is activated and inert triple bonds are broken. This is also true in Haber-Bosch process (HBP) as high performance catalysts are used to facilitate the electron transfer.[8-9] Among various reaction steps, the activation of N_2 is found to be the rate-determining step (RDS) in overall ammonia synthesis. However, recent works have shown that the RDS could be shifted from the dinitrogen dissociating activation to the adsorbed N specie's hydrogenation by utilizing electronic donors as substrates for Fe or Rh catalysts, especially electrides with low work functions, such as Li-H,[10] $12CaO{\cdot}7Al_2O_3$ (C12A7:e^-),[11-14] $[Y_5Si_3]^{0.79+}$:$0.79e^-$.[15-16] Detailed experiments and first-principle calculations revealed that negatively charged cobalt atoms in LaCoSi (400 °C, 0.1 MPa) can mediate the electrons from La to dinitrogen, dramatically lowering the activation barrier. Therefore, the active center with enriched electrons and low work function state is suggested to activate N_2 and facilitate the nitrogen fixation process.

Scheme 1 (A1) Schematic illustration of N_2 reduction process on nitrogenase; (A2) the structure of 1T MoS_2 and simulated Fe grafted onto 1T MoS_2

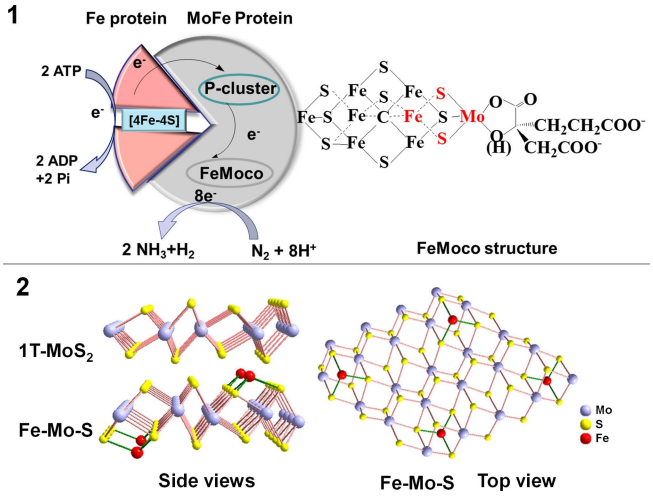

In nitrogenase, researchers have found that the coordination structure of Fe_7MoS_9C cluster plays a critical role in the activation of N_2.[7,17-21] Specially, Fe and Mo ions in asymmetrical Fe_7MoS_9C cluster are in near-tetrahedral and octahedral structure of hexahedral coordination geometry, respectively.[17,21-22] Various works to mimic nitrogenase also suggest the construction of asymmetrical coordinated metal atoms can realize higher NH_3 production.[23-24] For instances, Mo catalysts can reach the highest turnover number (TON) of 4350 equiv/Mo by utilizing a strong reducing reagent, SmI_2, as electrons donor.[25] Previously, freshly prepared FeS can react with N_2 and water to form ammonia with a yield of 0.1% per mole FeS.[26] The FeMoS-chalcogels built by symmetrical $[Mo_2Fe_6S_8]^{3+}$ and $[Sn_2S_6]^{4-}$ clusters show limited photocatalytic behavior in nitrogen fixation with a yield of ppm level, which is believed to result from its amorphous nature and symmetrical coordination of Fe and Mo.[27-28] Recently, density functional theory (DFT) calculations predicted that depositing Fe atoms on 2H-MoS_2 to form asymmetrical coordination of Fe, mimicking FeMo-co can spontaneously capture N_2 and show electrocatalytic behavior in reduction of N_2 at mild conditions.[29] Hence, combining both functional and structural bionic concepts, molecular engineering of materials with strong electron-donating properties and asymmetric coordinated active center to mimic-FeMo-co would be a promising way to achieve the N_2 activation at mild conditions.

Compared with 2H-MoS_2,[30-34] 1T-phase MoS_2 has enriched electron nature (low work function), but its thermodynamic instability restricts its broad applications.[35-37,38-40] Our previous work indicated Co and/or other transition metals can be grafted onto the S atoms at in-plane surface of octahedral 1T S-Mo-S layer *via* Co—S bonds to form an asymmetric coordinated Co active site, which can simultaneously enhance thermodynamic stability and electron density of 1T phase.[41] Based on these, a new class of N_2 fixation materials were constructed by replacing Co with Fe. Herein, asymmetrically coordinated Fe grafted on 1T MoS_2 as displayed in Scheme A2, was synthesized by a bottom-up method. The covalent bond characteristic of Fe—S is believed to improve the electron density and thermodynamic stability of the 1T MoS_2, and it can elevate the phase transition temperature to 450 °C. Notably, iron can act as an electron donor to lower work function. Due to the unique structure of enriched electrons nature and asymmetrical coordination, the obtained 1T $Fe_{0.1}Mo_{0.9}S_2$ layered material can directly react with water and dinitrogen to form ammonia with a yield of ~800 μmol (NH_4^+) g^{-1} (12.5% yield in mole, which is nearly 125 times of previous reported value[26]) at room temperature and atmosphere pressure without electricity or light.

Results and Discussion

Bottom-up synthesis of Fe grafted 1T MoS_2

1T MoS_2 and Fe-Mo-S materials were synthesized by utilizing $Na_2MoO_4{\cdot}2H_2O$ and S as raw materials and ethylene glycol as solvent *via* a solvothermal method (see Experimental section for details). 2H MoS_2 was synthesized for comparison *via* a hydrothermal process. Raman spectrum (Figure 1a) of the sample obtained from hydrothermal process shows strong and typical out-of-plane vibration A_{1g} (400 cm^{-1}) and E^1_{2g} (370 cm^{-1}) of trigonal prismatic (D_{3h}) coordination indicating the formation of hexagonal 2H MoS_2.[42] While, the Raman spectra of samples obtained with glycol as solvent presented significant changes. The typical J_1, J_2, J_3 vibration and in-plane vibration E^1_{1g} (283 cm^{-1}) derived from the MoS_6 octahedron (O_h) coordination reveal the formation of tetragonal 1T phase.[39,43]

The X-ray diffraction (XRD) patterns (Figure 1b) of layered Fe-Mo-S, 2H and 1T MoS_2 indicate low crystalline nature of these materials. Hexagonal 2H-MoS_2 synthesized with water as solvent

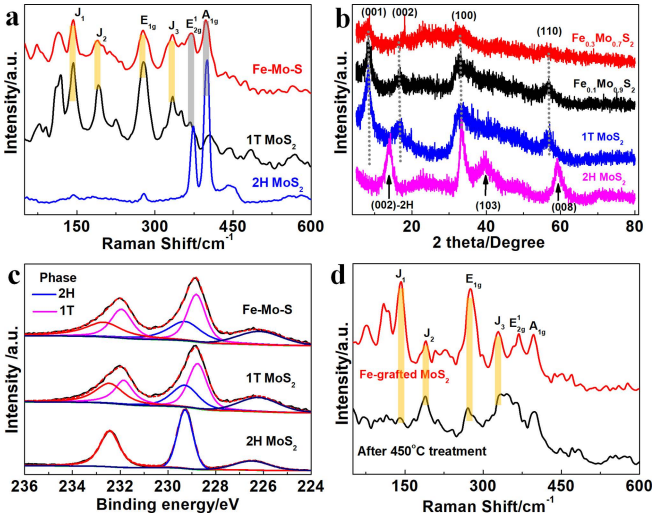

Figure 1 (a) Raman spectra, (b) XRD pattern, (c) XPS of Mo element in 2H, 1T-MoS_2 and Fe-Mo-S materials, (d) Raman of Fe-Mo-S materials before and after 450 °C treatment.

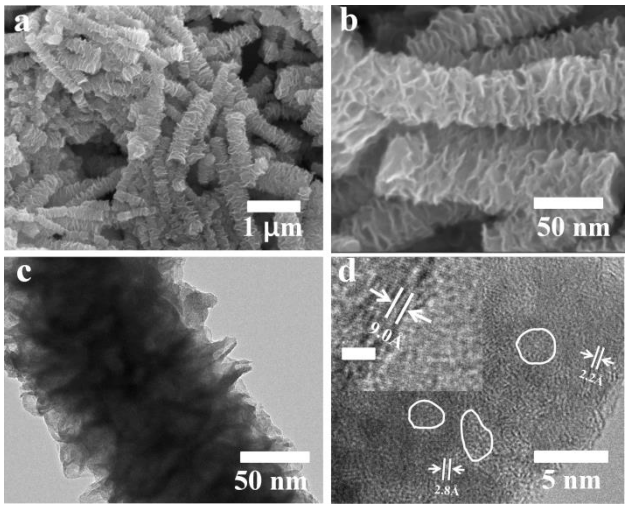

Figure 2 (a, b) SEM, (c) TEM and (d) HRTEM of $Fe_{0.1}Mo_{0.9}S_2$.

shows well stacked layered structure with a standard (002) plane of 2H-MoS_2 (JCPDS card No. 37-1492) at 14.7°, corresponding to an interlayer distance of 6.5 Å.[44-45] While the interlayer distance of samples (1T-MoS_2 and Fe-Mo-S) obtained in glycol system was enlarged to 9.0 Å (Figure 2d: Inset), resulting in two related (001) and (002) broad diffraction peaks around 8.1° and 16.8°, respectively.[32] Especially, 1T-MoS_2 and Fe-Mo-S materials display one characteristic diffraction peak derived from tetragonal (110) planes around 58°. The decreased intensity of Fe-Mo-S materials reveals the grafted Fe, leading to the distortion of tetragonal 1T structure and developing asymmetrical Fe—S coordination structure.[43] The molar ratio of Fe and Mo detected by inductively coupled plasma atomic emission spectrometry (ICP-AES) was 1 : 8.6 for $Fe_{0.1}Mo_{0.9}S_2$, which is close to the raw feeding ratio (Table S1).

The X-ray photoelectron spectroscopy (XPS) survey scan of $Fe_{0.1}Mo_{0.9}S_2$ material indicates the existence of Fe element (Figure S1). High resolution XPS spectra (Figure 1c) of Mo in 2H, 1T-MoS_2 and Fe-Mo-S materials reveal the valence state of Mo^{4+} according to 232.2 and 228.8 eV.[40] Meanwhile, compared with 2H-MoS_2, the Mo 3d in 1T-MoS_2 and Fe-Mo-S materials were shifted to low binding energy values revealing the formation of 1T phase with enriched available electrons. Differential scanning calorimetry (DSC, Figure S2) curve of Fe-Mo-S with only one broad peak around 150—200 °C is derived from the evaporation of H_2O and solvent (interlamellar H_2O molecule) indicating the good stability of 1T phase.[39] Raman (Figure 1d) spectrum of Fe-Mo-S after thermal treatment at 450 °C (Ar atmosphere, purity 99.99%) also displays the typical vibration J_1, J_2, J_3 of 1T-MoS_2 indicating the enhanced thermodynamic stability of 1T-MoS_2 by grafted Fe. Element mapping analysis of Fe-Mo-S materials presents uniform distribution of Fe atoms into 1T-MoS_2 (Figures S3 & S4). It's also worth noting that SEM and TEM images in Figures 2a, 2b and 2c show the Fe-Mo-S materials are layer-stacked hierarchical structures built by ultrathin nanosheets, which are different from 1T-MoS_2 (Figure S5). Moreover, the lattice fringes with 2.7 Å and 2.2 Å in the HRTEM image (Figure 2d) of $Fe_{0.1}Mo_{0.9}S_2$ plane nanosheets are corresponding to (100) and (110) of tetragonal 1T phase, respectively.[39,43] Some disordered amorphous areas (marked in white circles) can also be observed.

Nitrogen fixation behaviors

The performance of nitrogen fixation on obtained 1T Fe-Mo-S materials was investigated by multiple trails at room temperature and pressure atmosphere. As a result, the formation of ammonia was indeed observed when Fe-Mo-S materials directly reacted with water and dinitrogen at ambient conditions without external light or electricity. To avoid occasional result, the purification of N_2 gas and H_2O was carried out firstly, and controlled blank experiments were also performed before studying the dinitrogen fixation performance of designed Fe-Mo-S materials.[46-47] Detection of NH_4^+ ions was also carried out by different methods, including the Nessler and indophenol spectrophotometry, ion chromatography and ^1H NMR to ensure the generation of ammonia during the nitrogen-fixation process. The presence of NH_3 in solution was confirmed by the distinct green color released by the formation of indophenol dye after comparing with blank yellow aqueous solution (Figure 3a-1).[6,28] The Nessler reagent (Figure 3a-2) assay was also conducted, as another colorimetric way, it revealed the presence of ammonia in resulting solution by contrast with a blank (colorless) liquids.[6] For more accurate determination of ammonia production in this reaction, ^1H NMR spectra (Figure 3a) were recorded. The presence of NH_4^+ ions in the result solution was demonstrated according to the distinct triplet peaks in

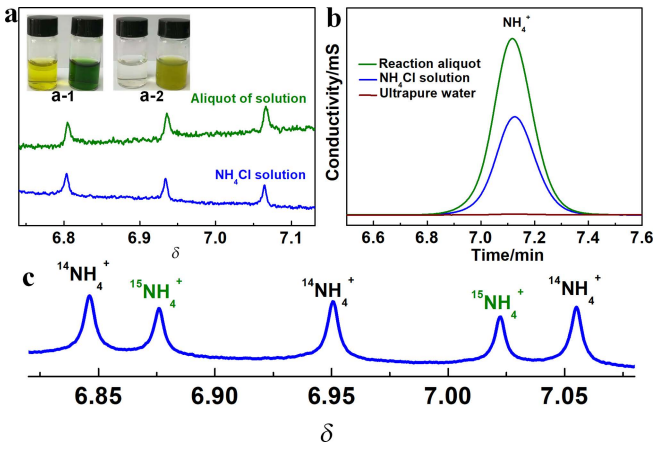

Figure 3 (a) Nuclear magnetic resonance spectra (H) of standard sample (NH_4Cl) and sample to be tested. (Insets, a-1, a-2) Photos of aliquots obtained during nitrogen-fixation process after performing the Nessler and indophenol colorimetric reactions (SI). (b) Representative ion chromatographs of aliquots obtained after nitrogen-fixation showing the presence of $[NH_4]^+$ ions. (c) Nitrogen source isotope analysis: the solution obtained by $Fe_{0.1}Mo_{0.9}S_2$ reacting with $^{15}N_2$.

^{1}H NMR. Furthermore, ion chromatography is also a direct method for detecting NH_4^+ ions (Figure 3b) with a retention time of NH_4^+ ions at ~7.2 min. To confirm whether N_2 gas is the source of NH_4^+ ions in the current system, isotopic labeling experiments were performed with air and $^{15}N_2$ gas (Figure 3c). ^{15}N isotope labelling experiment and corresponding ^{1}H NMR spectra indicate that the source of N element in generated NH_4^+ is indeed coming from the N_2 reduction process on Fe-Mo-S. Therefore, it is inferred that the generated NH_4^+ ions come from the reaction among Fe-Mo-S material, dinitrogen and water.

To further investigate the behavior of nitrogen fixation on Fe-Mo-S materials, different weights of $Fe_{0.1}Mo_{0.9}S_2$ were put into water to obtain various dispersions from 0.05 to 0.5 mg $Fe_{0.1}Mo_{0.9}S_2$ per milliliter water. The results were in good agreement with the cationic chromatographic analysis (Figure 4a) and the color change (Figure 4b) in the illustration. There is an approximately linear relationship between NH_4^+ ion concentration in the aqueous dispersion and the dosage of Fe-Mo-S materials as displayed in Figure 4c. Also, the yield by each gram of $Fe_{0.1}Mo_{0.9}S_2$ materials is nearly a constant, yield of ~280 μmol g^{-1} (4.1% yield in mole, in the initial 1 h). The system gave a fast generation rate of NH_4^+ in the initial 1 h, while nearly no more NH_4^+ will be formed after 4 h, and the NH_4^+ yield reached ~800 μmol (NH_4^+) g^{-1} (12.5% yield in mole) (Figure 4d). When air source was changed to the N_2 (99.99%) bubbling condition, the total amount of NH_4^+ ions increased to ~1000 μmol/g. The reproducibility of the reaction of $Fe_{0.1}Mo_{0.9}S_2$ materials with water under ambient conditions for 6 times (4 h) in parallel (Figure 4e) validated the performance of nitrogen fixation on Fe-Mo-S materials and ruled out this activity as an accidental result. In contrast, 2H-MoS_2 presented no ability

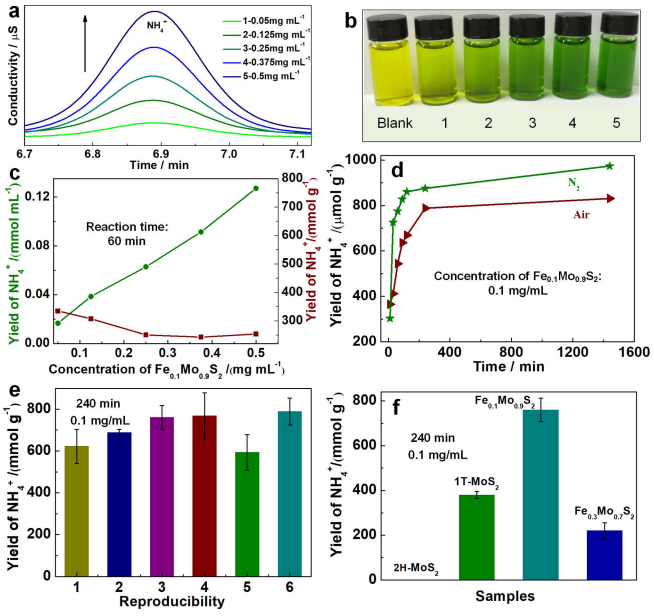

Figure 4 (a) Ion chromatography analysis of ammonia yield with concentration (Supporting Information and Figures S6—S10); (b) Illustration of indophenol colorimetric for NH_3 yield in different concentration of $Fe_{0.1}Mo_{0.9}S_2$ solutions; (c) Yield analysis of ammonia from two different perspectives (Reaction time = 60 min); (d) Nitrogen fixation performance (reaction time = 1440 min) of $Fe_{0.1}Mo_{0.9}S_2$ material (concentration = 0.1 mg/mL) under different gas bubbling condition (N_2 and Air); (e) Reproducibility of $Fe_{0.1}Mo_{0.9}S_2$ reaction with water at atmospheric pressure (reaction time = 240 min, concentration of materials = 0.1 mg/mL); (f) Different nitrogen fixation performances (reaction time = 240 min) of 2H-MoS_2, 1T-MoS_2 and the Fe-Mo-S (molar contents of iron: 10%, 30%) materials (concentration of materials = 0.1 mg/mL).

to convert N_2 to NH_4^+ in the previously mentioned system. The NH_4^+ yields of 1T MoS_2 and $Fe_{0.3}Mo_{0.7}S_2$ were 400 and 300 μmol/g (6.4% and 4.4% yield in mole), respectively (Figure 4f). It can be inferred that the yield of ammonia has the highest value on Fe-Mo-S materials when the 10% Fe was grafted onto 1T-MoS_2.

It could be clearly understood that only octahedron (O_h) structured 1T-materials have the ability of nitrogen fixation, which may be related to its unique enriched electronic structure and low work function properties, which implies the redox activities of materials. The work function of various materials was measured by UPS spectra. The original $Fe_{0.1}Mo_{0.9}S_2$ sample shows the smallest work function of 3.5 eV compared with 1T MoS_2 (4.05 eV) and $Fe_{0.3}Mo_{0.7}S_2$ (3.88 eV) (Figures S11 & S12). Low work function indicates the lower binding force of the material surface to electrons,[16] reflecting the layered Fe-Mo-S electron-rich compounds could serve as a favorable electron donors. These could offer available electrons to the lowest unoccupied molecular orbits of the N_2 molecule and active N≡N bonds. After reacting with water in air for 24 h, the work function of $Fe_{0.1}Mo_{0.9}S_2$ samples increased to 3.9 eV and nearly lost the ability to reduce N_2. These results demonstrate the nitrogen fixation process on Fe-Mo-S materials as a reactive-type process (A + B = C) rather than a catalytic process.

Theoretically, the 1T phase Fe-Mo-S material with enriched electrons feature offers its available electrons to nitrogen and water to form NH_4^+. EPR spectrum with a sharp signal at g = 2.00 (Figure S13) provides fingerprint evidence for the existence of free electrons in $Fe_{0.1}Mo_{0.9}S_2$ (like electrons in n-type semiconductor). The stronger EPR signal of $Fe_{0.1}Mo_{0.9}S_2$ dispersion (10 min) indicates that the $Fe_{0.1}Mo_{0.9}S_2$ has more free electrons, which were partially consumed during the process when reacting with water. High resolution XPS spectra (Figures S14—S16) of fresh-$Fe_{0.1}Mo_{0.9}S_2$ and used-$Fe_{0.1}Mo_{0.9}S_2$ samples show the slight shift of Fe 2p signals, indicating the Fe oxidation state is still the mixture of Fe^{2+} and Fe^{3+}. While the Mo3d (229.7, 233.1 eV), S2p (162.2, 162.6 eV) peaks shifted significantly to higher binding energy revealing that the available electrons are mainly stored in the 1T S-Mo-S frameworks, which is consistent with previous reports.[39] Besides the free electrons, the change of valance state of elements may also offer redox electrons for the formation of NH_3 and sides reductions of water, such as the generation of H_2 (Figure S26). All these electrons were measured as electron number by a classic iodometric method (Table S2).[12] The electron number of 1 T $Fe_{0.1}Mo_{0.9}S_2$ material changed from 19.4 to 14.9 mmol/g during the process, demonstrating that 4.5 mmol/g electrons were consumed to generate ammonia and other by-products. During this process, 1T $Fe_{0.1}Mo_{0.9}S_2$ material could utilize 53.3% of these electrons to generate ammonia with a yield of ~800 μmol/g NH_4^+ (12.5% yield in mole), which is much higher than 1T MoS_2 (38.0%) and $Fe_{0.3}Mo_{0.7}S_2$ (48.9%) and suggests the grafted Fe plays important actions on N_2 activation.

Nitrogen activation mechanism

To get deep insight about actions of Fe on activating N_2, the location and the specific coordination environment of Fe in Fe-Mo-S were further determined by X-ray absorption near-edge structure (XANES) and the extended X-ray absorption fine structure (EXAFS) of $Fe_{0.1}Mo_{0.9}S_2$ exposed in air.[48-49] XANES spectrum (Figure S17) revealed that the oxidization state of Fe in Fe-Mo-S is a mixture of Fe^{2+} and Fe^{3+}. Meanwhile, the comparison of Fourier-transformed EXAFS spectrum (Figure 5a) demonstrated that the first broad peak around 1.7 Å consists of three different bonds: Fe—N, Fe—O and Fe—S. Obviously, no Fe—Fe bond could be found in the obtained materials, showing clear dissimilarity from the spectrum of Fe foil. To further determine the position of Fe in coordinated structure, wavelet transformation and EXAFS fitting were carried out. Wavelet transformation (Figure 5b) showed two

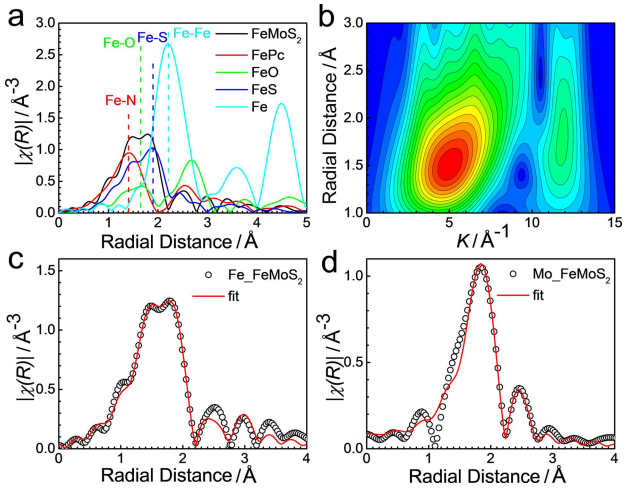

Figure 5 (a) Experimental Fe K-edge EXAFS spectra comparison of $Fe_{0.1}Mo_{0.9}S_2$, FePc (Iron phthalocyanine), FeO, FeS, (b) wavelet transform of experimental Fe K-edge EXAFS spectra of $Fe_{0.1}Mo_{0.9}S_2$, (c) best-fitted Fe K-edge EXAFS spectra of $Fe_{0.1}Mo_{0.9}S_2$ material, and (d) best-fitted Mo K-edge EXAFS spectra of $Fe_{0.1}Mo_{0.9}S_2$ material.

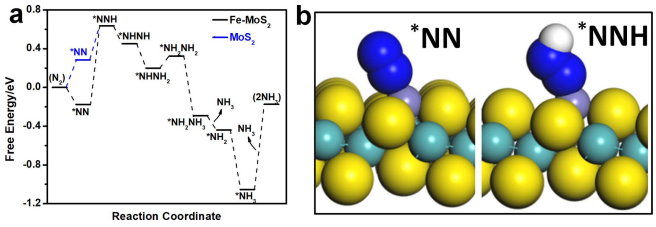

Figure 6 (a) The free energy profile of NRR on the basal plane of MoS_2 and that with one Fe atom doped. (b) The optimized structures of *NN and*NNH of Fe doped MoS_2 from DFT calculations. The colors are cyan for Mo, yellow for S, purple for Fe, blue for N, and white for H.

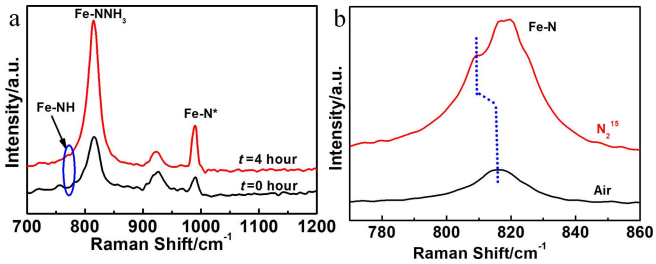

Figure 7 (a) Raman spectra from 750—860 cm^{-1} (The materials tested were obtained at 0 and 4 h of reacting with water and air, respectively), (b) Raman spectra of $Fe_{0.1}Mo_{0.9}S_2$ material treated with N_2^{15} and air atmosphere.

well separated peaks around 5 and 11 $Å^{-1}$ contributed by Fe—N as well as Fe—O, and Fe—S, respectively. While, Fe—N and Fe—O were hardly distinguished by EXAFS.[48] Hence, the model-based EXAFS fitting (Figure 5c) confirmed the mixed Fe—N, Fe—O and Fe—S in the $Fe_{0.1}Mo_{0.9}S_2$, which is in line with the FT-IR (Figure S18) and effectively verifies our assumption that Fe can facilely absorb N_2 and activate it in air condition. Meanwhile, the side reaction in present system may exist.

In addition, Mo and Fe EXAFS fitting (Figures 5c & 5d) could also confirm that Fe is grafted onto the surface of MoS_2 instead of substituting the bulk Mo. The fitting results indicated the Fe—Mo bonding length was around 3.12 Å (Figure S19 & Table S3), and the Mo—Mo bonding length was around 2.75 Å (Table S4). Besides, if Fe replaces the bulk Mo atoms, the Fe—Mo bonding length will be closer to Mo—Mo bonding length. Another evidence was that the Fe atoms only have 2 S coordinated with some N and O adsorbed, while the bulk Mo atoms have 6 S coordinated. The wavelet transfer of Mo K-edge EXAFS (Figures S20 & S21, Table S4) also confirmed only Mo—S bonding existing in the first shell, which does not have any N or O adsorbed as surface Fe atoms.

The successful identification of location and specific coordination environment of grafted Fe in Fe-Mo-S offers the opportunity to get deep understanding from theoretical simulation. DFT calculations were carried out to investigate the reaction pathway of N_2 reduction reaction (NRR) on both 1T MoS_2 and Fe grafted 1T MoS_2. Despite the growing interest in N_2RR, the reaction mechanism is still far from clear and in large dispute. In this work, we considered two possible reaction pathways: the associative distal (AD) pathway and the associative alternating (AA) pathway (SI). Previous research indicates that AA pathway is more favorable on both basal plane and edge of MoS_2.[44] With one Fe atom doped, we found that the AA pathway is more favorable, consistent with previous calculations.[44] The free energy profile of AA pathway on Fe doped MoS_2 is shown in Figure 6, while the free energy profile of AD (unfavorable) is shown in Figure S22. As shown in the free energy profile, *NNH formation is the potential determining step (PDS) with the formation energy of 0.81 eV. Compared with pure MoS_2, introducing Fe significantly increases the binding of N_2. Without Fe, MoS_2 shows no tendency to adsorb N_2 as indicated from the positive binding free energy of 0.34 eV, which mostly comes from the decreasing of entropy owing to adsorption. Instead, the presence of Fe significantly increases N_2 binding by −0.18 eV. Therefore, DFT calculation results suggest that the presence of Fe significantly increases the NRR performance by increasing N_2 binding, which is the first step towards N_2 reduction product.

We also predicted the vibrational frequencies of important reactive intermediates, such as Fe—N bonds in Fe—N* (1016 cm^{-1}), Fe—*N—NH_3 (815 cm^{-1}) and Fe—*NH (772 cm^{-1}) from DFT calculation, which can be directly compared with the experimental Raman spectra (Figure 7a) showing peaks at 990, 815 and 770 cm^{-1} (shoulder peak). The consistency between DFT calculations and experiment indicates the existence of possible reactive intermediate after introducing Fe, which demonstrated the important role of Fe site in NRR.

Besides the typical peaks of 1T MoS_2 and Fe—N species, vibration derived from Mo—N was clearly observed (Figure S23). The Mo—N bond is derived from the adsorption of N_2 on the S-Mo-S edge,[39,45] which is usually reported as active sites for NRR process. The abundant S-Mo-S edges may lead to the ability of 1T MoS_2 to active N_2. The intensity of Fe—N bond is significantly greater than those of the N—Mo bond and other peaks, indicating strong interactions between asymmetrical coordinated Fe and adsorbed N_2.

Based on theorical predictions, the isotope effect from ^{14}N to ^{15}N leads to wavenumber red shift of Fe—N vibrational mode. The activation of N_2 on the Fe-Mo-S was further studied by sealing the fresh material in isotopically labeled N_2^{15} gas for 72 h to perform free absorption. Generally, the formed covalent bonds of Fe—N^{14} are hardly to be exchanged with N_2^{15}. While labeled N_2^{15} gas would react with Fe-Mo-S and generate new Fe-N^{15} bonds. One can found a new Raman peak of Fe—N^{15} at 810 cm^{-1} (Figure 7b) can be observed besides the Fe—N^{14} peak at 815 cm^{-1}. The obvious red shift between Fe—N^{15} and Fe—N^{14} is consistent with the isotopic effect.[50] Different from covalent bond, the vibration of adsorbed N_2 should show a red shift single peak, which can be clearly observed in the Fourier Transform Infrared spectra (Figure S24). Therefore, it could be deduced that N_2 is easily adsorbed and activated on Fe in Fe-Mo-S material and then converted to

ammonia.

Based on all our results, the N_2 activation and reduction mechanism can be proposed as follows. Fe atoms were grafted onto 1T-MoS_2 *via* three Fe—S bonds during the solvothermal process based on previous report.[41] The unsaturated coordination of Fe grafted on 1T MoS_2 prefers to offer unoccupied 3d orbitals to adsorb and active N_2 to form serial Fe—N bond related species. The electron enriched 1T S-Mo-S framework at lower work function can offer its available electrons to meet with the energy request of N_2 reduction process. Driven by available electrons of $Fe_{0.1}Mo_{0.9}S_2$, the formed intermediate species can be further hydrogenated to produce NH_4^+ once unstable structure meets with missive water. After reacting with water and dinitrogen, the available electron density of materials and the ability of offering available electrons are decreased. Unfortunately, the adsorption free energy of O_2 on Fe atom site is –0.41 eV, which is (~0.27 eV) stronger than that of N_2 (Figure S25). Therefore, the side oxidation of Fe by O_2 and H_2O in $Fe_{0.1}Mo_{0.9}S_2$ material is also observed in the Fourier-transform infrared spectroscopy (FT-IR) spectra, and H_2 byproducts can also be detected during the N_2 reduction process (Figure S26).

Conclusions

In summary, inspired by the nitrogen fixation process on MoFe nitrogenase and developing industry of catalysts, asymmetrical coordinated Fe grafted onto 1T MoS_2 was successfully synthesized by a bottom-up method. The introduction of iron increased the electron density of materials and lowered work function rendering these materials as an electron donor. The unique enriched electronic and asymmetrical coordination structure made 1T $Fe_{0.1}Mo_{0.9}S_2$ layered material to actively react with water and N_2. Consequently, the formation of ammonia with a yield of ~800 μmol (NH_4^+) g^{-1} $Fe_{0.1}Mo_{0.9}S_2$ (12.5% yield in mole) at room temperature and atmosphere pressure was accomplished without electricity or light, which is greatly different from traditional bionic-inspired nitrogen fixation process. The fixation of N_2 was carefully investigated and confirmed by various isotopically labeled experiments. Moreover, the N_2 activation mechanism on Fe grafted 1T MoS_2 has also proposed based on the various controlling experiments, structure analysis based on XANES and EXAFS. The mechanism of the activation and reduction of N_2 was further investigated by DFT calculation and Raman spectra. It is believed the enriched electron nature of 1T MoS_2 structure and asymmetrical coordination of grafted Fe play key actions on the activation of dinitrogen on Fe-Mo-S materials at ambient condition. This work paves the potential way to develop highly electron utilization ratio nitrogen fixation materials for electro- or photo-NRR process *via* utilizing sustainable energy.

Experimental

All the experimental details can be found in Supporting Information.

Supporting Information

The supporting information for this article is available on the WWW under https://doi.org/10.1002/cjoc.202000675.

Acknowledgement

The work was supported by the Science and Technology Commission of National Natural Science Foundation of China (Nos. 21901156, 21975148 and 21771124), the Shanghai Municipality (Nos. 19JC1412600, 18QA1402400 and 18230743400). Z. Feng thanks the startup funding from Oregon State University. The XAS measurements were done at 9-BM of Advanced Photon Source, which is a U.S. Department of Energy (DOE) Office of Science User Facility operated for the DOE Office of Science by Argonne National Laboratory under Contract No. DE-AC02-06CH11357. T. Cheng and H. Yang thanks the Natural Science Foundation of Jiangsu Province (Grant No. SBK20190810), and the Jiangsu Province High-Level Talents (JNHB-106), the China Postdoctoral Science Foundation (No. 2019M660128), the Collaborative Innovation Center of Suzhou Nano Science & Technology, the Priority Academic Program Development of Jiangsu Higher Education Institutions (PAPD), and the 111 Project.

References

[1] Cui, X.; Tang, C.; Zhang, Q. A Review of Electrocatalytic Reduction of Dinitrogen to Ammonia under Ambient Conditions. *Adv. Energy Mater.* **2018**, *8*, 1800369.

[2] Chen, X.; Li, N.; Kong, Z.; Ong, W.-J.; Zhao, X. Photocatalytic fixation of nitrogen to ammonia: state-of-the-art advancements and future prospects. *Mater. Horiz.* **2018**, *5*, 9–27.

[3] Medford, A. J.; Hatzell, M. C. Photon-Driven Nitrogen Fixation: Current Progress, Thermodynamic Considerations, and Future Outlook. *ACS Catal.* **2017**, *7*, 2624–2643.

[4] Liu, Y.; Cheng, M.; He, Z.; Gu, B.; Xiao, C.; Zhou, T.; Guo, Z.; Liu, J.; He, H.; Ye, B.; Pan, B.; Xie, Y. Pothole-rich Ultrathin WO_3 Nanosheets that Trigger N identical withN Bond Activation of Nitrogen for Direct Nitrate Photosynthesis. *Angew. Chem. Int. Ed.* **2019**, *58*, 731–735.

[5] Krewald, V. Dinitrogen photoactivation: status quo and future perspectives. *Dalton Trans.* **2018**, *47* 10320–10329.

[6] Ithisuphalap, K.; Zhang, H.; Guo, L.; Yang, Q.; Yang, H.; Wu, G. Photocatalysis and Photoelectrocatalysis Methods of Nitrogen Reduction for Sustainable Ammonia Synthesis. *Small Methods* **2018**, *3*, 1800352.

[7] Foster, S. L.; Bakovic, S. I. P.; Duda, R. D.; Maheshwari, S.; Milton, R. D.; Minteer, S. D.; Janik, M. J.; Renner, J. N.; Greenlee, L. F. Catalysts for nitrogen reduction to ammonia. *Nat. Catal.* **2018**, *1*, 490–500.

[8] Ogawa, T.; Kobayashi, Y.; Mizoguchi, H.; Kitano, M.; Abe, H.; Tada, T.; Toda, Y.; Niwa, Y.; Hosono, H. High Electron Density on Ru in Intermetallic YRu_2: The Application to Catalyst for Ammonia Synthesis. *J. Phys. Chem. C* **2018**, *122*, 10468–10475.

[9] Schlogl, R. Catalytic synthesis of ammonia - A "never-ending story"? *Angew. Chem. Int. Ed.* **2003**, *42*, 2004–2008.

[10] Wang, P.; Chang, F.; Gao, W.; Guo, J.; Wu, G.; He, T.; Chen, P. Breaking scaling relations to achieve low-temperature ammonia synthesis through LiH-mediated nitrogen transfer and hydrogenation. *Nat. Chem.* **2017**, *9*, 64–70.

[11] Ye, T.-N.; Li, J.; Kitano, M.; Hosono, H. Unique nanocages of $12CaO{\cdot}7Al_2O_3$ boost heterolytic hydrogen activation and selective hydrogenation of heteroarenes over ruthenium catalyst. *Green Chem.* **2017**, *19*, 749–756.

[12] Kitano, M.; Kanbara, S.; Inoue, Y.; Kuganathan, N.; Sushko, P. V.; Yokoyama, T.; Hara, M.; Hosono, H. Electride support boosts nitrogen dissociation over ruthenium catalyst and shifts the bottleneck in ammonia synthesis. *Nat. Commun.* **2015**, *6*, 6731.

[13] Hasegawa, G.; Moriya, S.; Inada, M.; Kitano, M.; Okunaka, M.; Yamamoto, T.; Matsukawa, Y.; Nishimi, K.; Shima, K.; Enomoto, N.; Matsuishi, S.; Hosono, H.; Hayashi, K. Topotactic Synthesis of Mesoporous $12CaO{\cdot}7Al_2O_3$ Mesocrystalline Microcubes toward Catalytic Ammonia Synthesis. *Chem. Mater.* **2018**, *30*, 4498–4502.

[14] Hara, M.; Kitano, M.; Hosono, H. Ru-Loaded C12A7:e^- Electride as a Catalyst for Ammonia Synthesis. *ACS Catal.* **2017**, *7* 2313–2324.

[15] Lu, Y.; Li, J.; Tada, T.; Toda, Y.; Ueda, S.; Yokoyama, T.; Kitano, M.; Hosono, H. Water Durable Electride Y_5Si_3: Electronic Structure and Catalytic Activity for Ammonia Synthesis. *J. Am. Chem. Soc.* **2016**, *138*,

3970–3973.
[16] Gong, Y.; Wu, J.; Kitano, M.; Wang, J.; Ye, T.-N.; Li, J.; Kobayashi, Y.; Kishida, K.; Abe, H.; Niwa, Y.; Yang, H.; Tada, T.; Hosono, H. Ternary intermetallic LaCoSi as a catalyst for N_2 activation. *Nat. Catal.* **2018**, *1*, 178–185.
[17] Ohki, Y.; Uchida, K.; Tada, M.; Cramer, R. E.; Ogura, T.; Ohta, T. N_2 activation on a molybdenum-titanium-sulfur cluster. *Nat. Commun.* **2018**, *9* 3200.
[18] Morrison, C. N.; Spatzal, T.; Rees, D. C. Reversible Protonated Resting State of the Nitrogenase Active Site. *J. Am. Chem. Soc.* **2017**, *139*, 10856–10862.
[19] Brown, K. A.; Harris, D. F.; Rasmussen, A.; Khadka, N.; Hamby, H.; Keable, S.; Dukovic, G.; Peters, J. W.; Seefeldt, L. C.; King, P. W. B. Light-driven dinitrogen reduction catalyzed by a CdS-nitrogenase MoFe protein biohybrid. *Science* **2016**, *352*, 448–450.
[20] Anderson, J. S.; Rittle, J.; Peters, J. C. Catalytic conversion of nitrogen to ammonia by an iron model complex. *Nature* **2013**, *501*, 84–87.
[21] Spatzal, T.; Schlesier, J.; Burger, E. M.; Sippel, D.; Zhang, L.; Andrade, S. L.; Rees, D. C.; Einsle, O. Nitrogenase FeMoco investigated by spatially resolved anomalous dispersion refinement. *Nat. Commun.* **2016**, *7*, 10902.
[22] MacLeod, K. C.; Holland, P. L. Recent developments in the homogeneous reduction of dinitrogen by molybdenum and iron. *Nat. Chem.* **2013**, *5*, 559–565.
[23] Nishibayashi, Y. Nitrogen fixation: nitrido complexes step up. *Nat. Chem.* **2011**, *3*, 502–504.
[24] Arashiba, K.; Eizawa, A.; Tanaka, H.; Nakajima, K.; Yoshizawa, K.; Nishibayashi, Y. Catalytic Nitrogen Fixation via Direct Cleavage of Nitrogen-Nitrogen Triple Bond of Molecular Dinitrogen under Ambient Reaction Conditions. *B. Chem. Soc. Jpn.* **2017**, *90*, 1111–1118.
[25] Ashida, Y.; Arashiba, K.; Nakajima, K.; Nishibayashi, Y. Molybdenum-catalysed ammonia production with samarium diiodide and alcohols or water. *Nature* **2019**, *568*, 536–540.
[26] Dorr, M.; Kassbohrer, J.; Grunert, R.; Kreisel, G.; Brand, W. A.; Werner, R. A.; Geilmann, H.; Apfel, C.; Robl, C.; Weigand, W. *Angew. Chem. Int. Ed.* **2003**, *42*, 1540–1543.
[27] Liu, J.; Kelley, M. S.; Wu, W.; Banerjee, A.; Douvalis, A. P.; Wu, J.; Zhang, Y.; Schatz, G. C.; Kanatzidis, M. G. Nitrogenase-mimic iron-containing chalcogels for photochemical reduction of dinitrogen to ammonia. *Proc. Natl. Acad. Sci. U. S. A.* **2016**, *113*, 5530–5535.
[28] Banerjee, A.; Yuhas, B. D.; Margulies, E. A.; Zhang, Y.; Shim, Y.; Wasielewski, M. R.; Kanatzidis, M. G. Photochemical nitrogen conversion to ammonia in ambient conditions with FeMoS-chalcogels. *J. Am. Chem. Soc.* **2015**, *137*, 2030–2034.
[29] Azofra, L. M.; Sun, C. H.; Cavallo, L.; MacFarlane, D. R. Feasibility of N_2 Binding and Reduction to Ammonia on Fe-Deposited MoS_2 2D Sheets: A DFT Study. *Chem.-Eur. J.* **2017**, *23*, 8275–8279.
[30] Sun, T.; Li, Z.; Liu, X.; Ma, L.; Wang, J.; Yang, S. Oxygen-incorporated MoS_2 microspheres with tunable interiors as novel electrode materials for supercapacitors. *J. Power Sources* **2017**, *352*, 135–142.
[31] Zhang, L.; Li, M.; Zou, A.; Yu, S. H.; Xiong, T.; Wang, L.; He, J.; Fu, Q.; Sun, K.; Chua, D. H. C.; Xue, J. Synergistically Configuring Intrinsic Activity and Fin-Tube-Like Architecture of Mn-Doped MoS_2-Based Catalyst for Improved Hydrogen Evolution Reaction. *ACS Appl. Energy Mater.* **2018**, *2*, 493–502.
[32] Zhang, H.; Yu, L.; Chen, T.; Zhou, W.; Lou, X. W. D. Surface Modulation of Hierarchical MoS_2 Nanosheets by Ni Single Atoms for Enhanced Electrocatalytic Hydrogen Evolution. *Adv. Funct. Mater.* **2018**, *28*, 1807086.
[33] Xie, J.; Zhang, H.; Li, S.; Wang, R.; Sun, X.; Zhou, M.; Zhou, J.; Lou, X. W.; Xie, Y. Defect-rich MoS_2 ultrathin nanosheets with additional active edge sites for enhanced electrocatalytic hydrogen evolution. *Adv. Mater.* **2013**, *25*, 5807–5813.
[34] Ye, L.; Wu, C.; Guo, W.; Xie, Y. MoS_2 hierarchical hollow cubic cages assembled by bilayers: one-step synthesis and their electrochemical hydrogen storage properties. *Chem. Commun.* **2006**, 4738–4740.
[35] Druffel, D. L.; Kuntz, K. L.; Woomer, A. H.; Alcorn, F. M.; Hu, J.; Donley, C. L.; Warren, S. C. Experimental Demonstration of an Electride as a 2D Material. *J. Am. Chem. Soc.* **2016**, *138*, 16089–16094.
[36] Lin, Z.; Liu, Y.; Halim, U.; Ding, M.; Liu, Y.; Wang, Y.; Jia, C.; Chen, P.; Duan, X.; Wang, C.; Song, F.; Li, M.; Wan, C.; Huang, Y.; Duan, X. Solution-processable 2D semiconductors for high-performance large-area electronics. *Nature* **2018**, *562*, 254–258.
[37] Woods, J. M.; Jung, Y.; Xie, Y.; Liu, W.; Liu, Y.; Wang, H.; Cha, J. J. One-Step Synthesis of MoS_2/WS_2 Layered Heterostructures and Catalytic Activity of Defective Transition Metal Dichalcogenide Films. *ACS Nano* **2016**, *10*, 2004–2009.
[38] Zhang, N.; Surrente, A.; Baranowski, M.; Maude, D. K.; Gant, P.; Castellanos-Gomez, A.; Plochocka, P. Moiré Intralayer Excitons in a $MoSe_2/MoS_2$ Heterostructure. *Nano Lett.* **2018**, *18*, 7651–7657.
[39] Lei, Z.; Zhan, J.; Tang, L.; Zhang, Y.; Wang, Y. Recent Development of Metallic (1T) Phase of Molybdenum Disulfide for Energy Conversion and Storage. *Adv. Energy Mater.* **2018**, *8*, 1703482.
[40] Jia, W.; Zhou, X.; Huang, Y.; Cao, Y.; Sun, Y.; Jia, D. Synthesis of Air-stable 1T Phase of Molybdenum Disulfide for Efficient Electrocatalytic Hydrogen Evolution. *ChemCatChem* **2018**, *11*, 707–714.
[41] Li, X.; Zai, J.; Xiang, S.; Liu, Y.; He, X.; Xu, Z.; Wang, K.; Ma, Z.; Qian, X. Regeneration of Metal Sulfides in the Delithiation Process: The Key to Cyclic Stability. *Adv. Energy Mater.* **2016**, *6*, 1601056.
[42] Li, Y.; Zhang, H.; Jiang, M.; Kuang, Y.; Wang, H.; Sun, X. Amorphous Co–Mo–S ultrathin films with low-temperature sulfurization as high-performance electrocatalysts for the hydrogen evolution reaction. *J. Mater. Chem. A* **2016**, *4*, 13731–13735.
[43] Dong, H.; Xu, Y.; Zhang, C.; Wu, Y.; Zhou, M.; Liu, L.; Dong, Y.; Fu, Q.; Wu, M.; Lei, Y. MoS_2 nanosheets with expanded interlayer spacing for enhanced sodium storage. *Inorg. Chem. Front.* **2018**, *5*, 3099–3105.
[44] Zhang, L.; Ji, X.; Ren, X.; Ma, Y.; Shi, X.; Tian, Z.; Asiri, A. M.; Chen, L.; Tang, B.; Sun, X. Electrochemical Ammonia Synthesis via Nitrogen Reduction Reaction on a MoS_2 Catalyst: Theoretical and Experimental Studies. *Adv. Mater.* **2018**, *30*, 1800191.
[45] Sun, S.; Li, X.; Wang, W.; Zhang, L.; Sun, X. Photocatalytic robust solar energy reduction of dinitrogen to ammonia on ultrathin MoS_2. *Appl. Catal. B-Environ.* **2017**, *200*, 323–329.
[46] Andersen, S. Z.; Colic, V.; Yang, S.; Schwalbe, J. A.; Nielander, A. C. A rigorous electrochemical ammonia synthesis protocol with quantitative isotope measurements. *Nature* **2019**, *570*, 504–508.
[47] Hu, B.; Hu, M.; Seefeldt, L.; Liu, T. L. Electrochemical Dinitrogen Reduction to Ammonia by Mo_2N: Catalysis or Decomposition? *ACS Energy Lett.* **2019**, *4*, 1053–1054.
[48] Wang, M.; Árnadóttir, L.; Xu, Z. J.; Feng, Z. *In Situ* X-ray Absorption Spectroscopy Studies of Nanoscale Electrocatalysts. *Nano-Micro Lett.* **2019**, *11*, 47.
[49] Feng, Z.; Ma, Q.; Lu, J.; Feng, H.; Elam, J. W.; Stair, P. C.; Bedzyk, M. J. Atomic-scale cation dynamics in a monolayer VOX/α-Fe_2O_3 catalyst. *RSC Adv.* **2015**, *5*, 103834–103840.
[50] Chakravarty, S.; Kumar, N.; Panda, K.; Ravindran, T. R.; Panigrahi, B. K.; Dash, S.; Tyagi, A. K.; Amarendra, G. The influence of nitrogen concentration on microstructure and ultra-low friction behaviour of Fe–N thin films. *Tribol. Int.* **2014**, *74*, 62–71.

Manuscript received: December 15, 2020
Manuscript revised: March 2, 2021
Manuscript accepted: March 8, 2021
Accepted manuscript online: March 11, 2021
Version of record online: May 30, 2021

